

Journal of
Applied Remote Sensing

**Evaluating airborne hyperspectral
imagery for mapping saltcedar
infestations in west Texas**

Chenghai Yang
James H. Everitt
Reginald S. Fletcher

Evaluating airborne hyperspectral imagery for mapping saltcedar infestations in west Texas

Chenghai Yang,^a James H. Everitt,^b and Reginald S. Fletcher^c

^aUSDA-ARS Southern Plains Agricultural Research Center, 2771 F and B Road, College Station, Texas 77845

chenghai.yang@ars.usda.gov

^bRetired USDA-ARS Scientist, P.O. Box 8080, Weslaco, Texas 78599

^cUSDA-ARS, Crop Production Systems Research Unit, 141 Experimental Station Road, Stoneville, Mississippi 38776

Abstract. The Rio Grande River of west Texas contains by far the largest infestation of saltcedar (*Tamarix* spp.) in Texas. The objective of this study was to evaluate airborne hyperspectral imagery and different classification techniques for mapping saltcedar infestations. Hyperspectral imagery with 102 usable bands covering a spectral range of 475 to 845 nm was acquired from two sites along the Rio Grande in west Texas in December 2003 and 2004 when saltcedar was undergoing color change. The imagery was transformed using minimum noise fraction and then classified using six classifiers: minimum distance, Mahalanobis distance, maximum likelihood, spectral angle mapper, mixture tuned matched filtering, and support vector machine (SVM). Accuracy assessment showed that overall accuracy varied from 71% to 86% in 2003 and from 80% to 90% in 2004 for site 1 and from 60% to 76% in 2003 and from 77% to 91% in 2004 for site 2. The SVM classifier produced the highest overall accuracy, as well as the best user's and producer's accuracies for saltcedar among the six classifiers. The imagery taken in early December 2004 provided better classification results than that in mid-December 2003. Change detection analysis based on the classification maps quantified the class changes between the two years. These results indicate that airborne hyperspectral imagery incorporated with image transformation and classification techniques can be a useful tool for mapping saltcedar infestations. © 2013 Society of Photo-Optical Instrumentation Engineers (SPIE) [DOI: [10.1117/1.JRS.7.073556](https://doi.org/10.1117/1.JRS.7.073556)]

Keywords: airborne hyperspectral imagery; saltcedar; minimum noise fraction; mixture tuned matched filtering; support vector machine; change detection.

Paper 12465 received Dec. 18, 2012; revised manuscript received Apr. 24, 2013; accepted for publication Apr. 26, 2013; published online May 29, 2013.

1 Introduction

Saltcedar (*Tamarix* spp.), a perennial shrub or tree, was introduced to the United States from Europe and Asia in the 1800s for ornamental use and erosion prevention.¹ Although multiple species of saltcedar exist in the United States, the largest saltcedar invasion consists of two morphologically similar deciduous species, *Tamarix chinensis* and *Tamarix ramosissima*, and their hybrids.² These saltcedar species are invaders of riparian sites in the southwestern United States and northern Mexico and they form dense, low thickets that displace native plant communities, degrade wildlife habitat, increase soil salinity and wildfires, reduce water available for agriculture and municipalities, and reduce recreational use of affected areas.^{3,4} Saltcedar communities are also much less valuable for wildlife than the native riparian communities they displace.^{5,6}

Since saltcedar was introduced to the United States, it has escaped nearly all of its biological enemies and has proven difficult to control on a large scale by either manual or chemical methods.⁷ In recent years, biological control has been investigated as a mechanism for the control of

saltcedar. After extensive host-specificity testing, small leaf-feeding beetles (*Diorhabda* spp.) from the native range of saltcedar species in China and Kazakhstan were released and first established in Nevada, Utah, Colorado, and Wyoming to provide good control at little cost and with no damage to any other plants, while closely related *Diorhabda* beetles from Greece, Tunisia and Uzbekistan now are beginning to provide good biological control in Texas.^{8–12}

One of the important tasks for effective control of saltcedar is to map its distribution and quantify the infested areas. Remote sensing has the potential for this purpose. Several studies have been conducted on the use of remote sensing to distinguish saltcedar. Everitt and Deloach¹³ described the spectral light reflectance characteristics of saltcedar and demonstrated the use of normal color aerial photography for distinguishing infestations in Texas riparian areas. Everitt et al.¹⁴ used normal color aerial videography to detect and map saltcedar infestations on three river systems in the southwestern United States. More recently, Everitt et al.¹⁵ integrated aerial videography and photograph with global positioning system (GPS) and geographic information system technologies for mapping the distributions of saltcedar infestations along the Rio Grande River in west Texas and found that approximately 460 river-km of the Rio Grande from Lajitas to near El Paso was infested by saltcedar. Akasheh et al.¹⁶ used airborne multispectral digital imagery to map saltcedar and other riparian vegetation along the middle Rio Grande River in New Mexico and supervised classification results showed that multispectral imagery could accurately separate saltcedar from associated vegetation species with an overall accuracy of 88%. Narumalani et al.¹⁷ evaluated airborne imaging spectrometer for applications (AISA) hyperspectral imagery in conjunction with Interactive Self-Organizing Data (ISODATA) and spectral angle mapper (SAM) for mapping saltcedar in the Lake Meredith Recreational Area in Texas and accuracy assessment results showed that SAM (83%) provided a better accuracy than ISODATA (76%). More recently, Narumalani et al.¹⁸ used AISA hyperspectral imagery to map four dominant invasive plant species, including saltcedar, Russian olive, Canada thistle, and musk thistle along the flood plain of the North Platte River, Nebraska. Remote sensing is also a useful tool for assessing biological control of saltcedar. Anderson et al.¹⁹ successfully detected beetle-damaged saltcedar using compact airborne spectrographic imager (CASI) hyperspectral imagery in Nevada. Everitt et al.²⁰ also successfully identified saltcedar trees damaged by leaf-feeding beetles in Texas. Dennison et al.²¹ demonstrated the potential of advanced spaceborne thermal emission and reflection radiometer (ASTER) and moderate-resolution imaging spectroradiometer (MODIS) satellite data for monitoring defoliation caused by *Diorhabda* beetles in Utah.

Despite the success of mapping saltcedar in the reported studies, saltcedar classification from remotely sensed imagery is not always easy. In west Texas, saltcedar leafs out in mid-April and has a similar color to associate plant species, such as mesquite, during much of the year. However, mesquite will start defoliating in late November, while saltcedar changes from green to orange to yellow and then to a brown color before defoliation within a three- to four-week period from late November to late December.¹³ Therefore, it may be advantageous to use this unique phenology of saltcedar to distinguish it from associated plant species. The objectives of this study were to evaluate airborne hyperspectral imagery and different classification techniques for mapping saltcedar infestations during this phenological stage.

2 Methods

2.1 Study Area

Two representative study sites with mixed vegetation types, designated as site 1 and site 2, were selected from a saltcedar-infested area in Candelaria along the Rio Grande in west Texas. The longitude and latitude coordinates near the centers of the sites were (104°41'08" W, 30°06'53" N) for site 1 and (104°41'31" W, 30°07'50" N) for site 2. Saltcedar occurs in association with mixed woody species including western honey mesquite [*Prosopis glandulosa* var. *torreyana* (L. D. Benson) M. C. Johnst], seepwillow [*Baccharis salicifolia* (H. Ruiz Lopez and J. Pavon) C. Persoon], huisache [*Acacia minuate* (M. E. Jones) P. de Beauchamp], and mixed herbaceous species on both sites. There existed a large area of Bermuda grass (*Cynodondactylon* L.) at site 1 and patches of four-wing saltbush [*Atriplex canescens* (F. Pursh) T. Nuttall] were found along the river at site 2.

2.2 Acquisition of Hyperspectral Imagery

A hyperspectral imaging system described by Yang et al.²² was used to acquire images from the two sites. The system consisted of a digital CCD camera integrated with a hyperspectral filter and a PC equipped with a frame grabbing board and camera utility software. The camera was sensitive in the 280- to 1000-nm spectral range and has 1280(h) × 1024(v) pixels. The effective spectral range of the system was from 457.2 to 921.7 nm. The camera was configured to acquire 12-bit images with 128 spectral bands and a swath of 640 pixels.

A Cessna 404 twin-engine aircraft with a camera port in the floor was used as the platform for image acquisition. The hyperspectral imaging system was mounted on a light aluminum frame along with a three-camera multispectral imaging system. The three-camera system was used as a viewfinder to locate the target since the hyperspectral system captured one 640-pixel line at a time across the flight direction and did not provide a view of the imaging area. No stabilizer or inertial measurement device was used to dampen or measure platform variations, but care was taken to minimize the effects of winds and changes in the aircraft's speed and flight direction. The aircraft was stabilized at a predetermined altitude of 1980 m (6500 ft) above ground level, a speed of 178 km/h (110 miles/h), and a flight direction along the straight road within each site before the start of image acquisition and was maintained at the same altitude, speed, and direction during the course of image acquisition. A square ground pixel size of 1.56 m and a ground swath of 1000 m were achieved. Hyperspectral imagery was acquired between 1200 and 1300 h Central Standard Time on December 16, 2003, and December 1, 2004, under sunny and calm conditions.

2.3 Image Geometric Correction and Radiometric Calibration

The geometric distortions due to movements in the across-track direction and variations in roll were corrected using a reference line approach described by Yang et al.²² The geometrically restored hyperspectral images for the two sites were rectified to a geo-referenced QuickBird satellite image using a nonlinear rectification technique known as rubber sheeting. The satellite image was acquired on November 25, 2004 and rectified to the Universal Transverse Mercator (UTM), World Geodetic Survey 1984 (WGS-84), Zone 14, coordinate system based on a set of the ground control points located with a submeter-accuracy GPS Pathfinder Pro XRS receiver (Trimble Navigation Limited, Sunnyvale, California). For radiometric calibration, four 8-by-8-m tarpaulins with nominal reflectance values of 4%, 16%, 32%, and 48%, respectively, were placed in the study area during image acquisition. The actual reflectance values from the tarpaulins were measured using a FieldSpec HandHeld spectroradiometer (Analytical Spectral Devices, Inc., Boulder, Colorado). The spectroradiometer was sensitive in the visible to near-infrared (NIR) portion of the spectrum (325 to 1075 nm) with a spectral resolution of approximately 3 nm. The rectified hyperspectral images were converted to reflectance based on 128 calibration equations (one for each band) relating reflectance values to the digital count values on the four tarpaulins. All procedures for image rectification and calibration were performed using ERDAS IMAGINE (Intergraph Corporation, Madison, Alabama). Because the camera had low quantum efficiency near the NIR end of the observed spectrum, the reflectance values for wavelengths greater than 846 nm were not reliable. In addition, the first few bands in the blue region appeared to be noisy. Therefore, bands 1 to 5 and 108 to 128 (a total of 26 bands) were removed from each hyperspectral image and the remaining 102 bands were used for analysis.

2.4 Image Transformation, Classification and Accuracy Assessment

The minimum noise fraction (MNF) transformation implemented in ENVI (Research Systems, Inc., Boulder, Colorado) was used to reduce the spectral dimensionality and inherent spectral noise in the hyperspectral imagery.²³ Based on the eigen value plots and visual inspection of the MNF band images, the first 20 bands from the transformed MNF images were selected for image classification.²⁴

Based on ground observations, site 1 consisted of five major cover types, including saltcedar, mesquite mixed with small numbers of huisache and seepwillow species, Bermuda

grass, soil/sparse herbaceous species, and wet areas/water. Saltcedar and mesquite were the dominant woody species at site 1 and Bermuda grass occupied a significant portion of the site. Site 2 contained six major classes: dense saltcedar, sparse saltcedar, mixed woody species (mesquite, huisache, and four-winged saltbush), seepwillow, bare soil/sparse herbaceous species, and water. Saltcedar was the dominant woody species at site 2 and had two different levels of density. Continuous patches of seepwillow and four-winged saltbush also existed at this site. For supervised training, different numbers of areas, or regions of interest with known cover types were selected and digitized on each image as the training samples to represent respective classes or endmembers. These training areas were first verified on the ground with the aerial photographs and then selected on the hyperspectral images as training samples. The numbers of digitized training pixels ranged from 428 to 1934 among the classes for site 1 and from 83 to 3560 for site 2. A boundary was defined for each site to exclude the areas outside the boundary for image classification.

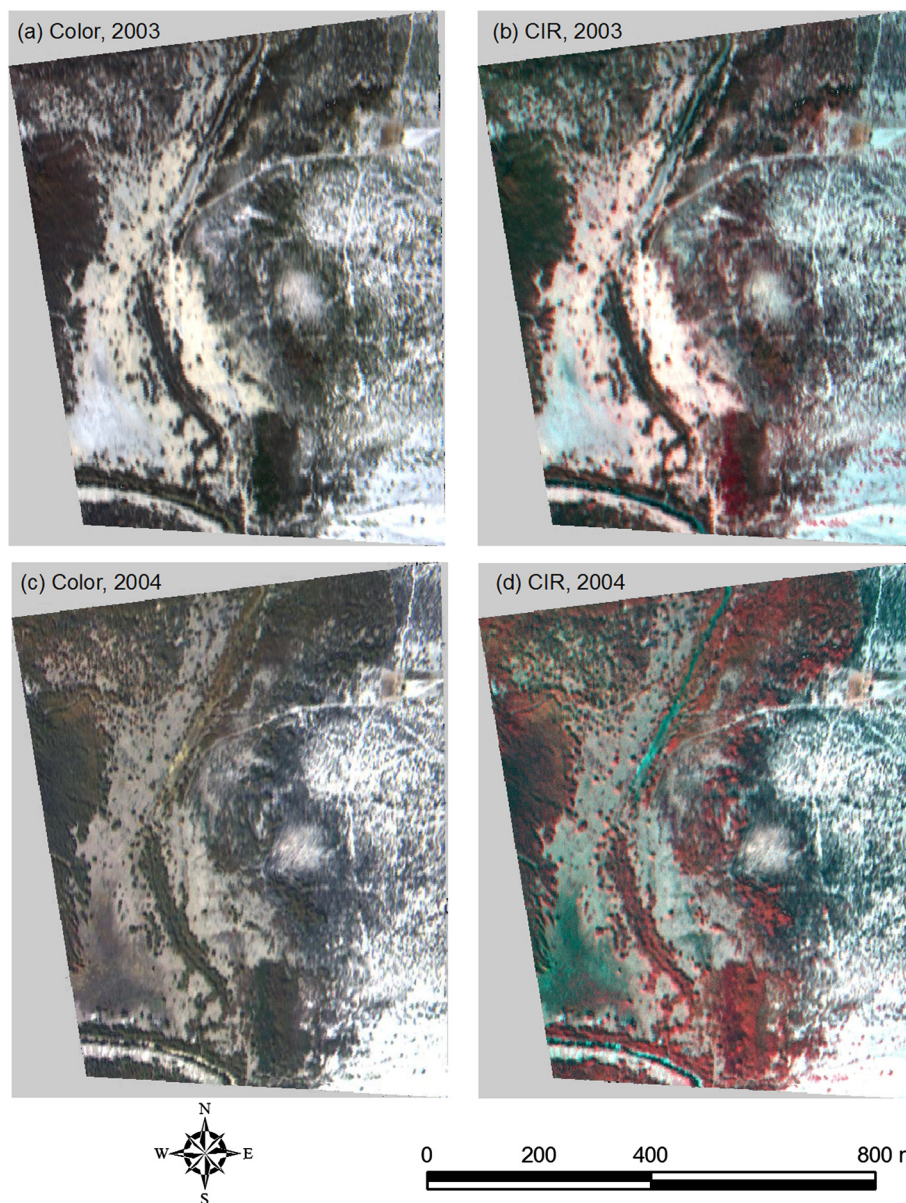


Fig. 1 Normal color and color-infrared (CIR) composite images derived from hyperspectral images taken in 2003 and 2004 for a saltcedar-infested site (site 1).

Six supervised classification methods including minimum distance, Mahalanobis distance (MAHD), maximum likelihood, SAM, mixture tuned matched filtering (MTMF), and support vector machine (SVM) were applied to the two MNF images. The minimum distance classifier uses the class means derived from the training data and assigns each pixel to the class that has the closest Euclidean distance from the pixel.²⁵ The MAHD method is similar to minimum distance, except that the covariance matrix is used in the calculation.²⁶ Each pixel is assigned to the class for which MAHD is the smallest. The maximum likelihood classifier calculates the probability that a given pixel belongs to a specific class and assigns the pixel to the class that has the highest probability.²⁷ MTMF is a spectral unmixing technique that maximizes the response of the defined endmembers on each endmember abundance image.²⁸ The matched filtering score images were classified into the classes based on maximum abundance values. The SAM classifier assigns pixels to the classes based on minimum spectral angles,²⁹ while the SVM classifier is a kernel-based machine learning technique that builds a model to predict which class a pixel belongs to.³⁰ The 2003 and 2004 MNF images for the two sites were classified using the six classification techniques. Since some of the classes at both sites were relatively small, they were merged to another class for accuracy assessment. The portions of the river at both study sites were narrow (4 to 7 m) and the trees growing along the banks of the river also covered part of the

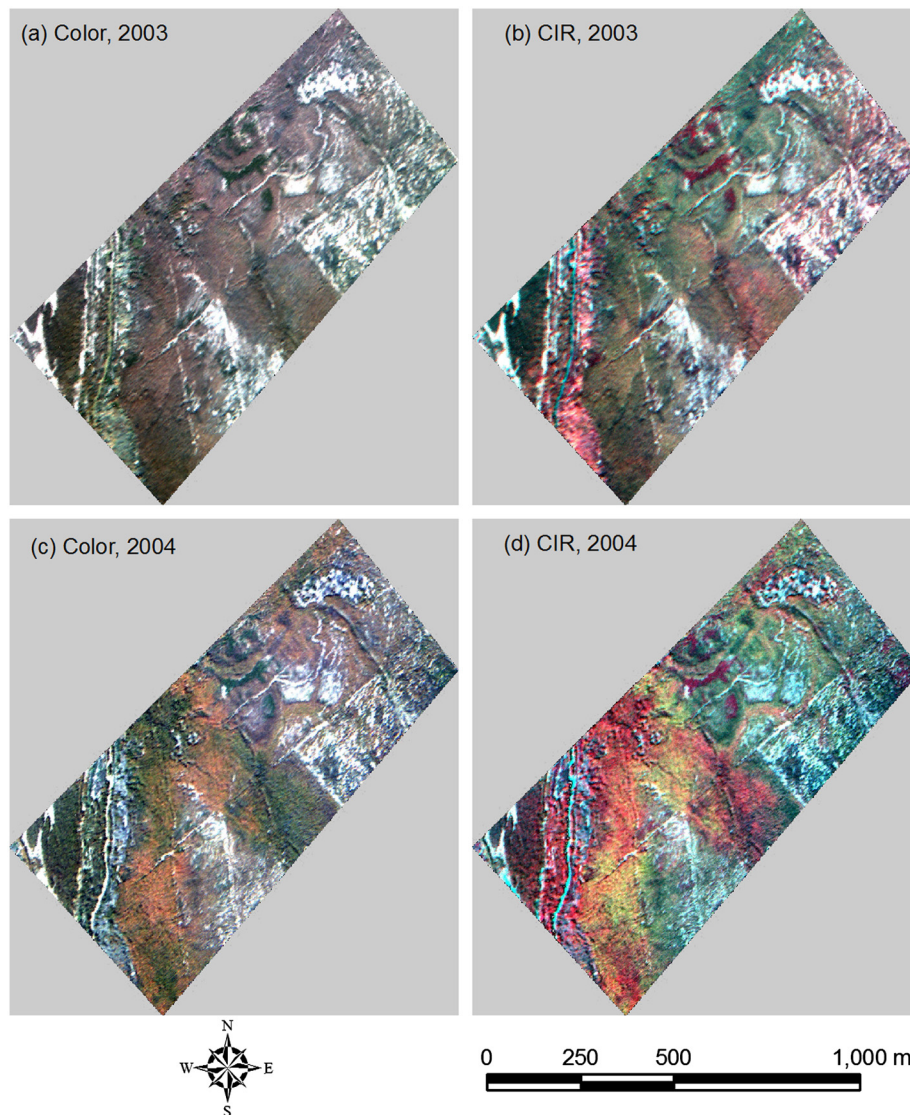


Fig. 2 Normal color and CIR composite images derived from hyperspectral images taken in 2003 and 2004 for a saltcedar-infested site (site 2).

river, resulting in small water surface areas. The wet areas change with rainfall. When it is dry, the wet areas become grass areas. Therefore, water and the wet areas at site 1 were merged with Bermuda grass as one class. At site 2, water was merged with bare soil/sparse herbaceous as a mixed class, and seepwillow was merged with other mixed woody species as one class. Thus, the classification maps for each site had four classes, though the four classes were different between the two sites.

For accuracy assessment of the merged classification maps, 100 points were generated and assigned to the classes in a stratified random pattern for each site. The UTM coordinates of these points were determined and the GPS receiver was used to navigate to these points for ground verification. Error matrices for each classification map were generated by comparing the classified classes with the actual classes at these points. Overall accuracy, producer's accuracy, user's accuracy, and kappa coefficients were calculated based on the error. Kappa analysis was also performed to test if each classification was significantly better than a random classification and if any two classifications were significantly different.³¹ Change detection analysis was performed on the classification maps to determine the class changes between the two years.

3 Results and Discussion

Figure 1 shows the normal color and color-infrared (CIR) composite images derived from the 102-band hyperspectral images taken in December 2003 and 2004 for site 1. By December, most of the mesquite trees had defoliated and most saltcedar changed color from green to yellow to brown. Therefore, mesquite looked dark green to dark brown on the color images and dark reddish on the CIR images, whereas saltcedar looks yellow green to dark brownish on the color

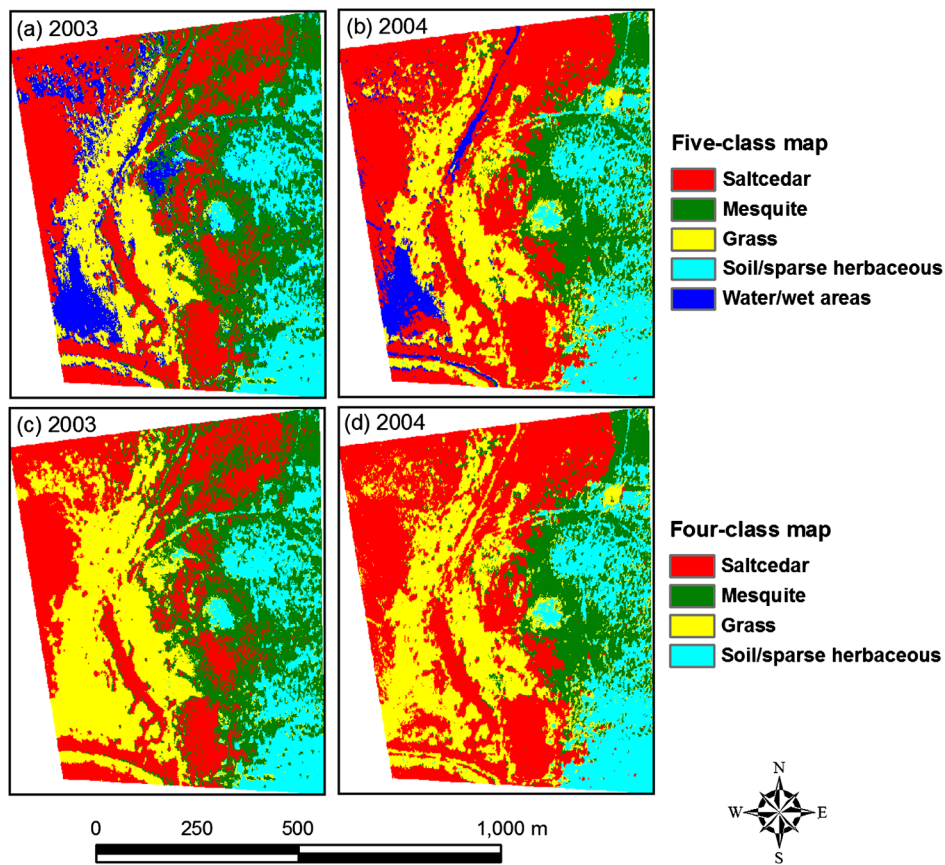


Fig. 3 Five-class classification maps generated from minimum noise fraction (MNF) images based on the support vector machine (SVM) classifier, as well as the four-class maps after the grass class and the water/wet areas class were merged for site 1.

images and dark to dark reddish on the CIR images. Most saltcedar already changed to brownish by December 16, 2003.

In comparison, most saltcedar were changing color from yellow to brown by December 1, 2004, while most mesquite trees had defoliated by this date. It appears that the early December image provided better separation between saltcedar and mesquite than the mid-December image. The best distinction between saltcedar and mesquite can be clearly seen on the 2004 CIR image. Bermuda grass and other herbaceous species were senesced and they had a grayish to whitish color on the images. The wet areas had a bluish tone on the CIR images.

Figure 2 shows the normal color and CIR composite images derived from the 102-band hyperspectral images taken in December 2003 and 2004 for site 2. Similarly, saltcedar looked brownish in 2003, while it had a green to orange tone in 2004. A few patches of seepwillow occurred near the northwest edge of the site. It looked dark green on the color image and dark red on the CIR image. Saltbush existed along the river close to the southwest corner of the site. It had a greenish and bluish color on the color image and a pinkish and reddish color on the CIR image.

Figure 3 presents the five-class classification maps from the 20-band MNF image based on the SVM classifier for site 1. The merged four-class maps are also shown in the figure. Similarly, Fig. 4 shows the six-class classification maps from the 20-band MNF images based on SVM as well as the merged four-class maps for site 2. A visual comparison of the classification maps with the color and CIR images indicates that the cover types at each site were generally well separated on these classification maps.

Table 1 summarizes the accuracy assessment results for the classification maps generated from the 20-band MNF images based on the six classification methods for site 1. Overall accuracy for 2003 was 71% for minimum distance, 75% for maximum likelihood, 76% for both SAM and MTMF, and 86% for SVM. Kappa analysis showed that all the classifications were

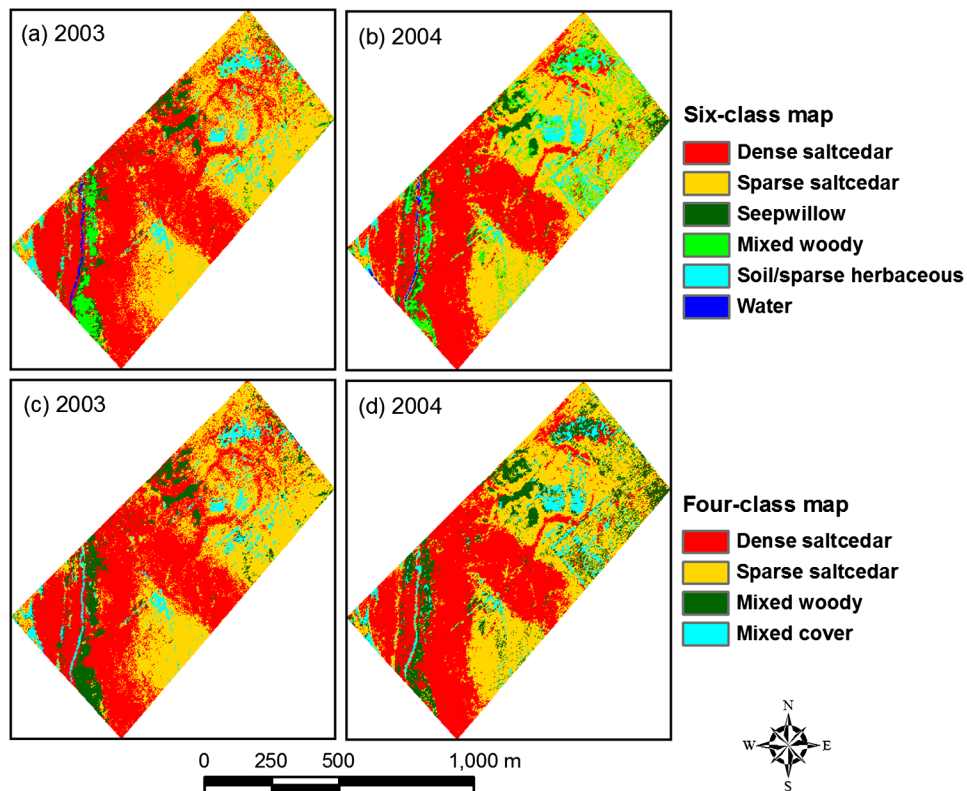


Fig. 4 Six-class classification maps generated from MNF images based on the SVM classifier, as well as the four-class maps after seepwillow and mixed woody species were merged as the mixed woody class and soil/sparse herbaceous species and water were merged as the mixed cover class for site 2.

Table 1 Accuracy assessment results for classification maps generated from minimum noise fraction (MNF) images based on six classification methods for site 1.

Year	Classifier ^a	Overall accuracy (%)	Overall kappa	Producer's accuracy (PA, %) and user's accuracy (UA, %)							
				Saltcedar		Mesquite		Grass		Soil/sparse herbaceous	
				PA	UA	PA	UA	PA	UA	PA	UA
2003	MD	79.0	0.718	63.4	96.3	94.4	50	91.7	91.7	82.4	93.3
	MAHD	71.0	0.597	73.2	81.1	61.1	40.7	91.7	84.6	47.1	80.0
	ML	75.0	0.663	61.0	92.6	77.8	53.9	91.7	75.9	82.4	77.8
	SAM	76.0	0.683	56.1	100.0	83.3	42.9	87.5	100.0	100.0	81.0
	MTMF	76.0	0.672	68.3	90.3	66.7	57.1	91.7	71.0	82.4	82.4
	SVM	86.0	0.805	87.8	92.3	77.8	70.0	91.7	84.6	82.4	93.3
2004	MD	86.0	0.805	87.8	97.3	77.8	73.7	95.8	76.7	76.5	92.9
	MAHD	89.0	0.847	87.8	97.3	77.8	87.5	95.8	82.1	94.1	84.2
	ML	87.0	0.821	82.9	97.1	72.2	86.7	95.8	82.1	100.0	77.3
	SAM	80.0	0.728	78.1	97.0	72.2	50.0	75.0	94.7	100.0	77.3
	MTMF	89.0	0.848	85.4	97.2	72.2	86.7	100.0	82.8	100.0	85.0
	SVM	90.0	0.861	90.2	97.4	72.2	81.3	100.0	88.9	94.1	84.2

^aMD = minimum distance, MAHD = Mahalanobis distance, ML = maximum likelihood, SAM = spectral angle mapper, MTMF = mixture tuned matched filtering, and SVM = support vector machine.

significantly better than a random classification and that SVM performed significantly better than the other five classifiers, which provided essentially the same overall accuracy. For 2004, SVM provided the highest overall accuracy (90%), followed by MAHD and MTMF (89%), maximum likelihood (87%), and SAM (80%). Between the two years, the 2004 imagery provided better classification results than the 2003 imagery. This was partially due the fact that the 2004 imagery was taken when saltcedar was still changing color from green to yellow to brown, while saltcedar already changed to brown in 2003. When saltcedar changes color to brown, it starts losing its leaves and has a dark brownish appearance similar to defoliated mesquite. Therefore, imagery should be taken before saltcedar changes to brown for better separation.

For 2003, SVM had a producer's accuracy of 88% and a user's accuracy of 92% for saltcedar and was the best classifier for differentiating saltcedar from the other cover types. The other five classifiers had good user's accuracy values of 81% to 100% and relatively low producer's accuracy values of 56% to 73% for the same year, indicating large areas of saltcedar were misclassified as the other cover types, especially as mesquite. For example, MTMF had a producer's accuracy of 68% and a user's accuracy of 90% for saltcedar. These values indicate that although 90% of the areas called saltcedar on the classification map were actually saltcedar, only 68% of the saltcedar areas on the ground were correctly identified as saltcedar on the map.

For 2004, SVM had a producer's accuracy of 90% and a user's accuracy of 97% for saltcedar and again was the best classifier for differentiating saltcedar from the other cover types. Minimum distance, MAHD, maximum likelihood and MTMF also had good producer's accuracy (83% to 89%) and excellent user's accuracy (97%) for saltcedar. In comparison, SAM had a lower producer's accuracy (78%) and a similar user's accuracy (97%) to the other five classifiers.

Table 2 summarizes the accuracy assessment results for the classification maps generated from the MNF images based on the six classifiers for site 2. Overall accuracy for 2003 ranged from a low of 60% for SAM to a high of 76% for SVM. Compared with site 1, site 2 had lower

Table 2 Accuracy assessment results for classification maps generated from MNF images based on six classification methods for site 2.

Year	Classifier ^a	Overall accuracy (%)	Overall kappa	Producer's accuracy (PA, %) and user's accuracy (UA, %)							
				Dense saltcedar		Sparse saltcedar		Mixed woody		Mixed cover	
				PA	UA	PA	UA	PA	UA	PA	UA
2003	MD	70.0	0.569	73.0	75.0	70.3	70.3	42.9	75.0	91.7	57.9
	MAHD	74.0	0.615	83.8	86.1	81.1	66.7	42.9	85.7	58.3	58.3
	ML	72.0	0.603	78.4	82.9	67.6	73.5	50.0	58.3	91.7	57.9
	SAM	60.0	0.411	48.7	90.0	81.1	50.0	35.7	83.3	58.3	50.0
	MTMF	73.0	0.613	81.1	88.2	73.0	71.1	42.9	66.7	83.3	52.6
	SVM	76.0	0.644	91.9	85.0	78.4	69.1	42.9	85.7	58.3	63.6
2004	MD	85.0	0.787	94.6	87.5	75.7	96.6	85.7	70.6	83.3	71.4
	MAHD	82.0	0.745	83.8	91.2	81.1	88.2	78.6	57.9	83.3	76.9
	ML	89.0	0.845	94.6	100.0	83.8	96.9	92.9	72.2	83.3	66.7
	SAM	77.0	77.0	81.1	93.8	82.4	70.0	56.3	75.0	76.9	62.5
	MTMF	79.0	0.700	86.5	94.1	81.1	83.3	100.0	53.9	25.0	75.0
	SVM	91.0	0.872	100.0	100.0	83.8	96.9	92.9	76.5	83.3	71.4

^aMD = minimum distance, MAHD = Mahalanobis distance, ML = maximum likelihood, SAM = spectral angle mapper, MTMF = mixture tuned matched filtering, and SVM = support vector machine.

Table 3 Kappa analysis results (Z-statistic) for pairwise comparisons among six classification maps generated from MNF images for site 1.

Year	Classifier	MD ^a	MAHD	ML	SAM	MTMF
2003	MAHD	1.48				
	ML	0.70	-0.78			
	SAM	0.46	-1.03	-0.25		
	MTMF	0.58	-0.88	-0.11	0.13	
	SVM	-1.20	-2.65 ^b	-1.89	-1.67	-1.76
2004	MAHD	-0.66				
	ML	-0.24	0.42			
	SAM	1.08	1.74	1.32		
	MTMF	-0.66	-0.01	-0.43	-1.75	
	SVM	-0.88	-0.23	-0.65	-1.97 ^b	-0.22

^aMD = minimum distance, MAHD = Mahalanobis distance, ML = maximum likelihood, SAM = spectral angle mapper, MTMF = mixture tuned matched filtering, and SVM = support vector machine.

^bSignificantly different between the two classifications at the 0.05 level ($Z \geq 1.96$). The negative sign indicates that the classifier on the left is better than the one on the top.

overall accuracy among the six classifiers. This was partially due to the confusion between dense saltcedar and sparse saltcedar. For 2004, SVM provided the highest overall accuracy (91%), followed by maximum likelihood (89%), minimum distance (85%) and MAHD (82%). SAM (77%) and MTMT (79%) had similar overall accuracy, but lower than the other classifiers. Again, the 2004 imagery provided better classification results than the 2003 imagery for site 2, partially due to the difference in imaging dates.

Tables 3 and 4 give the Kappa analysis results for pairwise comparisons among the six classification maps for sites 1 and 2, respectively. For site 1, SVM was significantly better than MAHD in 2003 and SAM in 2004, but there were no other significant differences among the classifiers. For site 2, SVM was significantly better than SAM in 2003 and SAM and MTMF in 2004. Moreover, MAHD and maximum likelihood were significantly better than SAM in 2003 and ML was significantly better than SAM and MTMF in 2004. These results

Table 4 Kappa analysis results (Z-statistic) for pairwise comparisons among six classification maps generated from MNF images for site 2.

Year	Classifier	MD ^a	MAHD	ML	SAM	MTMF
2003	MAHD	-0.51				
	ML	-0.38	0.14			
	SAM	1.67	2.19 ^b	2.07 ^b		
	MTMF	-0.49	0.02	-0.12	-2.19 ^b	
	SVM	-0.83	-0.32	-0.47	-2.53 ^b	-0.35
2004	MAHD	0.57				
	ML	-0.88	-1.45			
	SAM	1.47	0.90	2.35 ^b		
	MTMF	1.17	0.59	2.07 ^b	-0.32	
	SVM	-1.34	-1.90	-0.47	-2.80 ^b	-2.53 ^b

^aMD = minimum distance, MAHD = Mahalanobis distance, ML = maximum likelihood, SAM = spectral angle mapper, MTMF = mixture tuned matched filtering, and SVM = support vector machine.

^bSignificantly different between the two classifications at the 0.05 level ($Z \geq 1.96$). The negative sign indicates that the classifier on the left is better than the one on the top.

Table 5 Change detection statistics in terms of area (ha) between two classification maps based on support vector machine (SVM) for site 1.

		Initial state (2003)				
Class		Saltcedar	Mesquite	Grass	Soil/sparse herbaceous	Row total
Final state (2004)	Saltcedar	17.1	4.6	4.4	0.1	26.2
	Mesquite	1.7	7.2	0.6	1.3	10.8
	Grass	1.4	2.9	11.7	0.6	16.6
	Soil/sparse herbaceous	0.0	2.4	0.4	6.7	9.5
	Column total	20.2	17.1	17.1	8.7	
	Class change	3.1	9.9	5.4	1.9	
Image difference		6.0	-6.3	-0.5	0.8	

Table 6 Change detection statistics in terms of area (ha) between two classification maps based on SVM for site 2.

	Class	Initial state (2003)				Row total
		Dense saltcedar	Sparse saltcedar	Mixed woody	Mixed cover	
Final state (2004)	Dense saltcedar	23.7	3.7	1.7	0.4	29.5
	Sparse saltcedar	7.9	16.6	1.1	1.1	26.7
	Mixed woody	2.2	3.8	2.8	0.6	9.5
	Mixed cover	0.5	1.7	0.2	1.4	3.7
	Column total	34.3	25.8	5.8	3.5	
	Class change	10.6	9.2	3.0	2.1	
	Image difference	-4.8	1.0	3.6	0.2	

indicate that even though SVM performed better in most cases, most of the classifiers were similar. It is always a good practice to compare multiple classifiers so that best classifiers can be selected.

Tables 5 and 6 present the change detection statistics between the two best SVM-based classification maps for sites 1 and 2, respectively. The estimated area for saltcedar was 20.2 ha in 2003 and 26.2 ha in 2004, an increase of 6.0 ha. For the 20.2 ha of saltcedar identified in 2003, 17.1 ha remained to be saltcedar, but 1.7 and 1.4 ha of the saltcedar was classified as mesquite and grass, respectively, in 2004. Moreover, 4.6 of mesquite, 4.4 ha of grass and 0.1 ha of soil/sparse herbaceous vegetation identified in 2003 were classified as saltcedar in 2004. Some of these class changes were attributed to the natural changes of the classes, while some were simply due to misclassifications in both years, especially in 2003. For site 2, the estimated area decreased from 34.3 to 29.5 ha of dense saltcedar and increased from 25.8 to 26.7 ha for sparse saltcedar. Again, the class changes were attributed to actual changes and misclassifications. It is not always easy to separate saltcedar from surrounding vegetation and the timing of the image acquisition is very critical. Change detection results can be affected by the accuracy of the classification maps. This factor needs to be taken into consideration in interpreting the temporal changes.

4 Conclusions

The results from this study demonstrate that airborne hyperspectral imagery incorporated with image transformation and classification techniques can be a useful tool for mapping saltcedar infestations. Among the six classification methods examined in this study, SVM performed the best in both years for both sites. The other five classifiers provided good classifications in some cases, but they were not consistent. Between the two imaging dates, the early December, 2004 imagery provided better classification results than the mid-December, 2003 imagery, indicating the sensitivity and importance of phenology for saltcedar identification. For better separation, the imagery should be taken when saltcedar is undergoing the color change, but before it turns to brown. This unique phenological stage only lasts only three to four weeks in west Texas. The optimum imaging time may vary from year to year depending on the weather conditions. Therefore, it is necessary to investigate the possibility to distinguish saltcedar from the time it starts leafing out to the time it starts defoliating. Hyperspectral imagery in conjunction with advanced image processing techniques may offer the potential for mapping saltcedar during other times of the growing season. This study was the first study for evaluating airborne hyperspectral imagery for identifying saltcedar in west Texas and provides useful information for further research on the use of multispectral and hyperspectral imagery for mapping saltcedar infestations along the Rio Grande.

Acknowledgments

The authors thank Rene Davis (retired USDA-ARS pilot) and Fred Gomez of USDA-ARS at College Station, Texas, for image acquisition and Jim Forward of U.S. Fish and Wildlife Service at Alamo, Texas, for assistance in image rectification and ground verification. We also thank Harry Miller and Martin Kennedy and their associates for allowing us to use their ranch for this study. Disclaimer: Mention of trade names or commercial products in this article is solely for the purpose of providing specific information and does not imply recommendation or endorsement by the U.S. Department of Agriculture (USDA), which is an equal opportunity provider and employer.

References

1. B. R. Baum, "Introduced and naturalized tamarisks in the United States and Canada (Tamaricaceae)," *Baileya* **15**(1), 19–25 (1967).
2. J. F. Gaskin and B. A. Schaal, "Molecular phylogenetic investigation of U.S. invasive Tamarix," *Syst. Bot.* **28**(1), 86–95 (2003), <http://dx.doi.org/10.1043/0363-6445-28.1.86>.
3. J. M. DiTomaso, "Impact, biology, and ecology of saltcedar (*Tamarix* spp.) in the Southwestern United States," *Weed Technol.* **12**(2), 326–336 (1998).
4. C. J. DeLoach et al., "Host specificity of the leaf beetle, *Diorhabda elongata deserticola* (Coleoptera: Chrysomelidae) from Asia, a biological control agent for saltcedars (Tamarix: Tamaricaceae) in the western United States," *Biol. Contr.* **27**(2), 117–147 (2003), [http://dx.doi.org/10.1016/S1049-9644\(03\)00003-3](http://dx.doi.org/10.1016/S1049-9644(03)00003-3).
5. T. A. Kerpez and N.S. Smith, *Saltcedar control for wildlife habitat improvements in the southwestern United States*, Res. Pub. 169, p. 16, USDI, U.S. Fish and Wildlife Serv., Washington, DC (1989).
6. C. J. DeLoach, "Prospects for biological control of saltcedar (*Tamarix* spp.) in the riparian habitats of the southwestern United States," in *Proc. VII Int. Symp. Biol. Contr. Weeds*, E. S. Delfosse, Ed., pp. 307–314, Instituto Sperimentale per la Patologia Vegetale, Ministero dell' Agricoltura e delle Foreste, Rome, Italy (1990).
7. C. J. DeLoach et al., "Ecological interactions in the biological control of saltcedar (*Tamarix* spp.) in the United States: toward a new understanding," in *Proc. 10th Int. Symp. Biol. Contr. Weeds*, N. R. Spencer and R. Nowierski, Eds., pp. 819–873, Montana State University, Bozeman, Montana (2000).
8. P. A. Lewis et al., "Assessment of risk to native Frankenia shrubs from an Asian leaf beetle, *Diorhabda elongata deserticola* (Coleoptera: Chrysomelidae), introduced for biological control of saltcedars (*Tamarix* spp.) in the western United States," *Biol. Contr.* **27**(2), 148–166 (2003), [http://dx.doi.org/10.1016/S1049-9644\(03\)00004-5](http://dx.doi.org/10.1016/S1049-9644(03)00004-5).
9. P. A. Lewis et al., "Biology of *Diorhabda elongata deserticola* (Coleoptera: Chrysomelidae), an Asian leaf beetle for biological control of saltcedars (*Tamarix* spp.) in the United States," *Biol. Contr.* **27**(2), 101–116 (2003), [http://dx.doi.org/10.1016/S1049-9644\(03\)00002-1](http://dx.doi.org/10.1016/S1049-9644(03)00002-1).
10. J. L. Hudgeons et al., "Establishment and biological success of *Diorhabda elongata* on invasive Tamarix in Texas," *Southwest. Entomol.* **32**(3), 157–168 (2007), <http://dx.doi.org/10.3958/0147-1724-32.3.157>.
11. R. I. Carruthers et al., "Saltcedar areawide pest management in the western United States," in *Areawide Pest Management: Theory and Implementation*, O. Koul, G. Cuperus, and N. Elliott, Eds., pp. 252–279, CAB International, Wallingford, UK (2008).
12. C. J. DeLoach et al., *Progress on Biological Control of Saltcedar in Texas 2004–2008*, USDA, Agr. Res. Serv., Temple, Texas (2009).
13. J. H. Everitt and C.J. DeLoach, "Remote sensing of Chinese tamarisk (*Tamarix chinensis*) and associated vegetation," *Weed Sci.* **38**(3), 273–278 (1990).
14. J. H. Everitt et al., "Using spatial information technologies to map Chinese tamarisk (*Tamarix chinensis*) infestations," *Weed Sci.* **44**(1), 194–201 (1996).
15. J. H. Everitt et al., "Remote mapping of saltcedar in the Rio Grande system of west Texas," *Texas J. Sci.* **58** (1), 13–22 (2006).
16. O. Akasheh, C. Neale, and F. Farag, "Spatial mapping of riparian vegetation in the middle Rio Grande River, New Mexico," in *Proc. 19th Biennial Workshop on Color Photography*,

- Videography, and Airborne Imaging in Resource Assessment*, American Society Photogrammetry and Remote Sensing, Bethesda, Maryland, CDROM (2004).
17. S. Narumalani et al., "A comparative evaluation of ISODATA and spectral angle mapping for the detection of saltcedar using airborne hyperspectral imagery," *Geocarto Int.* **21**(2), 59–66 (2006), <http://dx.doi.org/10.1080/10106040608542384>.
 18. S. Narumalani et al., "Detecting and mapping four invasive species along the floodplain of North Platte River, Nebraska," *Weed Technol.* **23**(1), 99–107 (2009).<http://dx.doi.org/10.1614/WT-08-007.1>
 19. G. L. Anderson et al., "Monitoring the dynamics of saltcedar biological control in Lovelock, Nevada," in *Proc. 19th Biennial Workshop on Color Photography, Videography, and Airborne Imaging in Resource Assessment*, American Society Photogrammetry and Remote Sensing, Bethesda, Maryland, CDROM (2004).
 20. J. H. Everitt et al., "Using remote sensing to assess biological control of saltcedar," *Southwest. Entomol.* **32**(2), 93–103 (2007), <http://dx.doi.org/10.3958/0147-1724-32.2.93>.
 21. P. E. Dennison et al., "Remote monitoring of tamarisk defoliation and evapotranspiration following saltcedar leaf beetle attack," *Rem. Sens. Environ.* **113**(7), 1462–1472 (2009), <http://dx.doi.org/10.1016/j.rse.2008.05.022>.
 22. C. Yang et al., "A CCD camera-based hyperspectral imaging system for stationary and airborne applications," *Geocarto Int.* **18**(2), 71–80 (2003), <http://dx.doi.org/10.1080/10106040308542274>.
 23. A. A. Green et al., "A transformation for ordering multispectral data in terms of image quality with implications for noise removal," *IEEE Trans. Geosci. Rem. Sens.* **26**(1), 65–74 (1988), <http://dx.doi.org/10.1109/36.3001>.
 24. C. Yang, J. H. Everitt, and H. B. Johnson, "Applying image transformation and classification techniques to airborne hyperspectral imagery for mapping Ashe juniper infestations," *Int. J. Rem. Sens.* **30**(11), 2741–2758 (2009), <http://dx.doi.org/10.1080/01431160802555812>.
 25. J. B. Campbell, *Introduction to Remote Sensing*, 3rd ed., Guilford Press, New York (2002).
 26. ERDAS, *ERDAS Field Guide*, ERDAS, Inc., Norcross, Georgia (2010).
 27. J. A. Richards, *Remote Sensing Digital Image Analysis*, Springer-Verlag, Berlin (1999).
 28. J. C. Harsanyi and C. I. Chang, "Hyperspectral image classification and dimensionality reduction: an orthogonal subspace projection approach," *IEEE Trans. Geosci. Rem. Sens.* **32**(4), 779–785 (1994), <http://dx.doi.org/10.1109/36.298007>.
 29. F. A. Kruse et al., "The spectral image processing system (SIPS): interactive visualization and analysis of imaging spectrometer data," *Rem. Sens. Environ.* **44**(2–3), 145–163 (1993), [http://dx.doi.org/10.1016/0034-4257\(93\)90013-N](http://dx.doi.org/10.1016/0034-4257(93)90013-N).
 30. C.-W. Hsu, C.-C. Chang, and C.-J. Lin, "A practical guide to support vector classification," National Taiwan University, Taipei, <http://ntu.csie.org/~cjlin/papers/guide/guide.pdf> (10 May 2013).
 31. R. G. Congalton and K. Green, *Assessing the Accuracy of Remotely Sensed Data: Principles and Practices*, Lewis Publishers, Boca Raton, Florida (1999).

Biographies and photographs of the authors not available.